

Active Tension Network model of epithelial mechanics

Nicholas Noll,¹ Madhav Mani,^{2,3} Idse Heemskerk,³ Sebastian Streichan,³ and Boris I. Shraiman^{1,3}

¹*Department of Physics, University of California Santa Barbara*

²*Northwestern University Applied Math*

³*Kavli Institute for Theoretical Physics*

It is now widely recognized that mechanical interactions between cells play a crucial role in epithelial morphogenesis, yet understanding the mechanisms through which stress and deformation affect cell behavior remains an open problem due to the complexity inherent in the mechanical behavior of cells and the difficulty of direct measurement of forces within tissues. Theoretical models can help by focusing experimental studies and by providing the framework for interpreting measurements. To that end, “vertex models” have introduced an approximation of epithelial cell mechanics based on a polygonal tiling representation of planar tissue. Here we formulate and analyze an Active Tension Network (ATN) model, which is based on the same polygonal representation of epithelial tissue geometry, but in addition i) assumes that mechanical balance is dominated by cortical tension and ii) introduces tension dependent local remodeling of the cortex, representing the active nature of cytoskeletal mechanics. The tension-dominance assumption has immediate implications for the geometry of cells, which we demonstrate to hold in certain types of *Drosophila* epithelial tissues. We demonstrate that stationary configurations of an ATN form a manifold with one degree of freedom per cell, corresponding to “isogonal” - i.e. angle preserving - deformations of cells, which dominate the dynamic response to perturbations. We show that isogonal modes account for $\sim 90\%$ of experimentally observed deformation of cells during the process of ventral furrow formation in *Drosophila*. Other interesting properties of our model include the exponential screening of mechanical stress and a negative Poisson ratio response to external uniaxial stress. We also provide a new approach to the problem of inferring local cortical tensions from the observed geometry of epithelial cells in a tissue.

I. INTRODUCTION

Mechanics of growth and cellular rearrangements plays an important role in morphogenesis as both processes are central to defining the shape of developing tissues. As such, it has become a subject of intense study aiming to characterize specific mechanical processes involved in cell and tissue-wide dynamics [1–4], uncover the regulatory mechanisms [5], and identify if and how the mechanical state of the cell feeds back onto the larger developmental program [6–9]. Yet at the present, these questions remain largely unanswered due to the difficulty of measuring mechanical stress in live tissues and the challenge of identifying the relevant sub-cellular degrees of freedom needed to model the cell’s mechanical state.

Many developmental processes involve two-dimensional epithelial layers, making it essential to understand cell mechanics in such systems. In its simplest form, an epithelial tissue is a monolayer of apico-basally polarized cells tightly connected to their lateral neighbors [10]. Viewed from the apical side, cells tessellate the plane, forming a polygonal packing reminiscent of a soap foam. Unlike passive foams, interfacial tension is not a simple material property, but rather derives from the cortical

actin-myosin network [11, 12] localized as a planar ring just inside the cell’s lateral surface [13]. Each cell’s cortical cytoskeleton is linked to those of the neighboring cells via adherens junctions [14]. The equilibrium geometry of cells is determined by the balance of cytoskeletal forces [5, 15] within the tissue. However, unlike passive materials, cells actively regulate such forces through mechanotransduction and internal remodeling, resulting in an intrinsically time-dependent stress-strain constitutive relation and controllable plasticity [16, 17], which can drive rearrangement of cells. Elucidation of the manner in which cellular activity manifests in collective properties of the tissue is critical to understanding morphogenesis.

Here we formulate a phenomenological model of an epithelial tissue as a two dimensional Active Tension Network (ATN), which in addition to cytoskeletal elasticity describes cytoskeletal re-arrangement through myosin activity and the recruitment of myosin into cytoskeletal fibers, thus capturing the plastic response of cells to external stress. We shall demonstrate that the assumption that mechanical equilibrium of cells is dominated by tension has testable consequences for cell and tissue morphology, allowing immediate tests of this hypothesis. We show that Active Tension Networks have a number

of interesting mechanical properties, which include “screening” that (exponentially) localizes transient perturbations. Furthermore, an ATN’s ground state is degenerate: a consequence of the fact that “isogonal” - i.e. angle preserving - perturbations of cell geometry also preserve tension balance. These isogonal (zero) modes dominate ATN fluctuations and result in unusual behaviors in response to external perturbations. For example, we demonstrate that an ATN generates a negative Poisson ratio in response to a uniaxial stress. We also provide a new *local* “Mechanical Inverse” [18, 19] algorithm for inferring cytoskeletal tension - under the ATN approximation - from images of epithelial tissue. Finally, we shall demonstrate that dynamics of the initial stage of *Drosophila* Ventral Furrow formation is well described by the ATN model.

II. RESULTS

A. Formulation of the Active Tension Net Model

Epithelial cell monolayers form approximate two-dimensional polygonal tilings, that are conveniently parameterized by the set of vertex coordinates $\{\mathbf{r}_i\}$. The mechanical state of the tissue is often described using a generalized ‘Vertex Model’ [2, 8, 20] which defines the mechanical energy of a cell array (given by vertex positions $\{\mathbf{r}_i\}$ connected by edges defined by the array’s topology) as

$$E = \sum_{\langle i,j \rangle} \frac{\kappa_{ij}}{2} (r_{ij} - \ell_{ij})^2 + \sum_{\alpha} \frac{\kappa'_{\alpha}}{2} (A_{\alpha} - \bar{A}_{\alpha})^2 \quad (1)$$

which incorporates the cortical cytoskeleton contributions from each interface ij - elastic energy stored by deformation of the bundle’s length, r_{ij} , relative to its intrinsic length, ℓ_{ij} , as well as the mechanical energy associated with cell area, A_{α} , deformation relative to the intrinsic area \bar{A}_{α} . Anticipating the heterogeneity of cells, Eq. (1) allows for the variation of intrinsic parameters from cell to cell and interface to interface. However, it is useful to further generalize the description by defining mechanical energy in its differential form [18]

$$dE[\{\mathbf{r}_i\}] = \sum_{\langle i,j \rangle} T_{ij} dr_{ij} + \sum_{\alpha} p_{\alpha} dA_{\alpha} \quad (2)$$

Here tension T_{ij} defines the change in mechanical energy in response to the change of edge length by dr_{ij} and ‘pressure’ (or more precisely, radial stress

in cylindrical coordinates) p_{α} defines the response to the change in area by dA_{α} . The force acting on a vertex is simply the projection of the above energy differential along the corresponding vertex displacement - i.e. $\mathbf{F}_i \equiv -\partial_{\mathbf{r}_i} E$.

Equation (2) is more general than (1): the mechanical degrees of freedom $\{T_{ij}\}$ and $\{p_{\alpha}\}$ provide the means to describe the full time dependent behavior of a heterogeneous cell array, beyond the constitutive relations implied by Eq. (1). Instead of considering this model in its full generality, we will make the simplifying assumption that the contribution of ‘pressure’ to mechanical balance can be neglected in comparison to tension. This is tantamount to the assumption that the magnitude of typical pressure differentials across cell interfaces satisfies $\Delta p \ll \bar{T}/\bar{r}$, where \bar{T} and \bar{r} are the characteristic scales of tension and length of an interface respectively. This implies that the interfacial curvature $\Delta p/\bar{T}$ - as defined by the Young-Laplace law [18, 21] - is small compared to cellular length scales and thus this assumption is appropriate for any epithelial cell array with little to no observable bond curvature. As such, we set $p_{\alpha} = p_0$ and convert the sum over cell areas to a boundary condition on the change of total tissue area, $p_0 \sum dA_{\alpha}$. In this limit, the only forces within the bulk of the cell array are interfacial tensions due to cortical acto-myosin and the pressure only enforces conservation of the total area of the cell array, preventing its collapse under the action of internal tension. Alternatively, we will be considering finite patches of tissue with specified normal stresses on the boundary (that also prevent collapse), as a boundary condition. We shall refer to the corresponding structures as ‘Tension Nets’ and investigate their properties in some detail.

Dynamics of vertex positions within a tension net is assumed to be relaxational

$$\nu \frac{d}{dt} \mathbf{r}_i = -\partial_{\mathbf{r}_i} E = \sum_{\{j\}_i} T_{ij} \hat{\mathbf{r}}_{ji} \quad (3)$$

where $\{j\}_i$ denotes the set of all vertices connected to vertex i and ν represents the effective friction between apical cytoskeleton and its substrate [22]; it sets the timescale of mechanical relaxation, assumed to be fast relative to morphogenetic time scales. We adopt the constitutive relation for tension corresponding to the cortical contribution to mechanical energy given in Eq. (1)

$$T_{ij} = \kappa(r_{ij} - \ell_{ij}) \quad (4)$$

where for simplicity we assumed homogeneous cytoskeletal stiffness, $\kappa_{ij} = \kappa$, effectively setting the

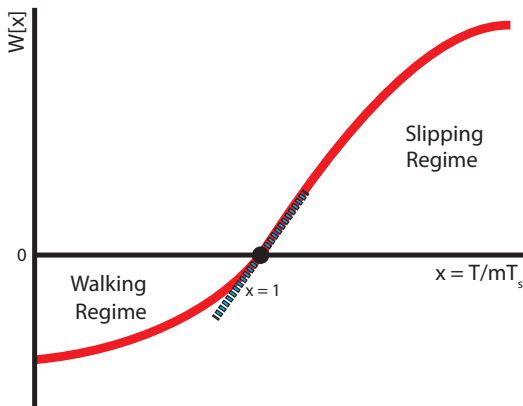


FIG. 1. Expected dependence of the local contractility rate of the cortical acto-myosin filament on the mechanical load, $W(x)$ - hereafter referred to as the "walking kernel". The generic features are the zero crossing at $x = 1$ which separates myosin activity into a regime of walking, $W(x) < 0$, and slipping, $W(x) > 0$, and the positive slope, $W'(x = 1) > 0$ - i.e. we slip above the stall force. The dynamics close to the fixed point is immune to the exact functional form (which are cell-specific) and will only measure the aforementioned slope - depicted as a dashed blue line.

scale of tension. However, as already mentioned above, acto-myosin bundles are not simple passive elastic elements, but can dynamically remodel in response to external stimuli [23]. In the simplest form this remodeling can be described by letting the intrinsic length of each intercellular edge ℓ_{ij} evolve dynamically on a time scale slow compared to the mechanical relaxation of the tissue described by Eq. (3). Specifically:

$$\frac{d}{dt}\ell_{ij} = \ell_{ij}W\left(\frac{T_{ij}}{m_{ij}T_s}\right) \quad (5)$$

where $W\left(\frac{T_{ij}}{m_{ij}T_s}\right)$ describes the dependence of the local contractility rate of the cortical acto-myosin filament on the mechanical load T_{ij} that it carries. The generic features of W are known from single-molecule experiments [24, 25]: each myosin will walk in a polarized direction, contracting the actin bundle, unless the load per myosin, T_{ij}/m_{ij} , reaches the "stall force" level T_s . Above this critical value, the filament simply elongates as each motor slips backwards [26]. We note that in assuming the load carried by each myosin motor scales inversely proportional with the total number of motors, we have

implicitly assumed that motors are non-interacting which is only valid for low densities [27].

Given a specified myosin distribution on interfaces, Eqs. (3 – 5) define the dynamics of an active tension net. The fixed point of these equations is then reached when i) tensions balance at all vertices and ii) all edges are at their stall force, set by the local myosin level. Alas, arbitrarily specified myosin levels will lead to a frustrated system where these conditions cannot be satisfied. Indeed not all distributions of tensions under fixed topology will admit a set of angles that balance in the plane. However, in reality myosin levels are not fixed and are known to themselves respond to cytoskeletal tension through mechanotransduction [9, 28]. Here we shall propose a particular form of mechanical feedback on myosin, that will ensure convergence to a balanced state. Specifically, we assume that myosin is locally recruited into acto-myosin fibers under positive strain rate of the intrinsic length:

$$\frac{d}{dt}m_{ij} = \frac{\mu m_{ij}}{\ell_{ij}} \frac{d\ell_{ij}}{dt} = \mu m_{ij}W\left(\frac{T_{ij}}{m_{ij}T_s}\right) \quad (6)$$

with μ parameterizing the speed of myosin recruitment; myosin redistribution occurs on morphogenetic timescales and thus the postulated feedback is assumed to occur slow relative to both mechanical relaxation and acto-myosin contractility. While presently we do not have direct evidence for this specific form of mechanical feedback on local myosin concentrations, it is generally consistent with experimental observations [9, 28].

B. Static properties of Tension Nets

The force balance condition of a static tension net defines equilibrium geometry through Eq. (7)

$$\mathbf{F}_i = \sum_{\{j\}_i} T_{ij}\hat{\mathbf{r}}_{ji} = 0 \quad (7)$$

This immediately defines a relationship, for the ratio of tensions of any pair of adjacent edges in terms of angles at their shared vertex (depicted in Fig. 2(a)).

$$\frac{T_{ij}}{T_{il}} = \frac{\hat{\mathbf{r}}_{il} \wedge \hat{\mathbf{r}}_{ik}}{\hat{\mathbf{r}}_{ik} \wedge \hat{\mathbf{r}}_{ij}} \quad (8)$$

Since the product of such ratios computed for any closed loop of edges has to be equal to unity, a consistent global assignment of tensions $\{T_{ij}\}$ is only possible if the polygonal array satisfies the following

each dual vertex must sum to 2π , which imposes c constraints on tensions, that are the dual of the compatibility constraints on the geometry of the original cell array. The existence of these constraints implies that an arbitrary distribution of myosin concentrations would not allow mechanical equilibration and thus motivates our conjectured mechanical feedback on myosin dynamics. The existence of a dual triangulation for equilibrium tension nets also provides a robust way of inferring tensions from experimentally observed cell array geometries, improving on the previously proposed ‘‘Mechanical Inverse’’ method [18, 19].

C. Variational approach to inferring tension from the geometry of a Tension Net.

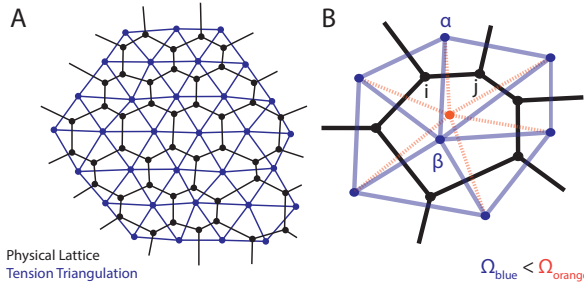


FIG. 3. (a) Graphical example of a static tension net, shown in black, and its corresponding tension triangulation or dual graph, shown in blue. (b) Cartoon illustrating the variational inverse. Algorithm projects observed tissue geometry onto the ‘closest’ tension triangulation. Blue is the better fit of the two shown.

Provided the lattice obeys the compatibility constraint globally, the force balance condition defines a local mechanical inference method based on ‘‘propagating’’ Eq. (8) for ratios of tensions, along adjacent edges. This local method is convenient insofar as it allows inference independent of boundary conditions. In practice, however, as seen in Fig. 2(c), the compatibility constraint is at best only approximately satisfied. Thus the direct use of Eq. (8) would result in an accumulation of errors as geometric factors are multiplied together. To circumvent this problem we define a more general variational method which finds the best fit tension graph - i.e. position of the vertices of the corresponding triangulation - to the observed epithelial geometry by minimizing the (pseudo-) energy functional defined

by

$$\Omega[\{\mathbf{Q}_\alpha^*\}, \Lambda|\{\hat{\mathbf{r}}_{ij}\}] = \frac{1}{2} \sum_{\langle \alpha, \beta \rangle} [(\mathbf{Q}_\alpha^* - \mathbf{Q}_\beta^*) \cdot \hat{\mathbf{r}}_{\alpha\beta}]^2 - \frac{\Lambda}{2} \sum_{\langle \alpha, \beta \rangle} (\mathbf{Q}_\alpha^* - \mathbf{Q}_\beta^*)^2 \quad (10)$$

where $\hat{\mathbf{r}}_{\alpha\beta}$ is the unit vector along the common edge of neighboring cells α and β . We constrain the variance of tension $\mathbf{T}_{\alpha\beta}$ to be equal to one via Lagrange multiplier Λ to preclude the trivial solution. Variation of the above functional with respect to dual vertices returns

$$\frac{\delta \Omega}{\delta \mathbf{Q}_\alpha^{*a}} = \sum_{\{\beta\}_\alpha} \left[\hat{\mathbf{r}}_{\alpha\beta}^a \hat{\mathbf{r}}_{\alpha\beta}^b - \Lambda \delta^{ab} \right] [\mathbf{Q}_\alpha^{*b} - \mathbf{Q}_\beta^{*b}] \quad (11)$$

where $\{\beta\}_\alpha$ denotes the set of all cells adjacent to cell α . Λ is chosen to be the smallest value that ensures the matrix defined by Eq. (11) has a non-trivial null space; it measures the deviation of the epithelial geometry from a true static tension net insofar that it is a necessary global perturbation to the orthogonality condition between an edge and its dual conjugate. Fig. 3(b) illustrates the action of this algorithm: minimization of Ω amounts to minimizing the overlap between all edges and their conjugate duals.

Equations (10,11) reduce the tension inference problem to convex minimization subject to quadratic constraints and thus can be numerically solved using interior point methods standard to Quadratically Constrained Quadratic Programming (QCQP) [35]. The benefit of the proposed variational ‘‘Mechanical Inverse’’ method is that the output is a true static tension net - the algorithm projects the observed lattice onto the closest static tension net and extracts tension parameters from the projection. Provided the tissue snapshot can be thought of as a static tension net with superimposed fluctuations, representing real dynamical fluctuations plus measurement errors, the variational inverse algorithm should provide a more robust measurement of equilibrium parameters as compared to the matrix inversion of force balance equations done on instantaneous tissue geometry [18, 19].

D. Multiplicity of equilibrium Tension Net geometries.

Next we observe that the number of degrees of freedom for equilibrium tension net geometries,

given by at $2v - c = 3c$ (v being the number of vertices of the cell array), is larger than the $2c$ degrees of freedom for the dual triangulations of the tension plane. Hence, a given set of tensions must correspond to multiple possible polygonal arrays: specifically, to a manifold of nets with one degree of freedom per cell. To sort this out we first note that our construction of the dual triangulation generalizes the standard passage from the Voronoi lattice to its Delaunay dual triangulation. Conversely, given a triangulation we can construct a dual polygonal lattice by defining the circumcenter for each triangle and drawing a Voronoi lattice based on these centroids. Yet, such a lattice is not the unique dual of the tension triangulation. As long as none of the vertex angles are perturbed, we can freely “inflate” or “deflate” lattice cells, as illustrated in Fig. 4(a), without disturbing mechanical equilibrium and thus the underlying tension-triangulation. The compatibility condition satisfied by equilibrium nets is essential for allowing such “isogonal” - i.e. angle preserving - dilation modes to exist.

This mathematical observation has interesting physical implications, as it suggests that “isogonal” deformations should dominate observed fluctuations of tension nets close to mechanical equilibrium, acting as easily excitable “soft modes” of the cellular lattice. Moreover, we expect that the isogonal modes are fundamental to ATN dynamics on time scales longer than mechanical equilibration, but short compared to the redistribution of myosin. Because tension net equilibrium (at static cortical myosin) does not specify a unique cell array geometry, after any transient perturbation from equilibrium a cell array is not constrained to relax to the original configuration, but instead moves to a different point on the c -dimensional isogonal manifold. Fig. 4(b) illustrates the expected long-term dynamics. The result is a very particular form of “plasticity” which should be manifest in the tissue’s dynamics. As such, we now examine dynamics of an ATN close to the equilibrium.

E. Dynamical properties of Active Tension Nets.

The dynamics near equilibrium is most naturally expressed in terms of edge vectors $\mathbf{r}_{\alpha\beta}$, where each edge is labeled by the cells it partitions, in this case cells α, β . In this representation, one must enforce the geometric constraint that edge vectors sum to

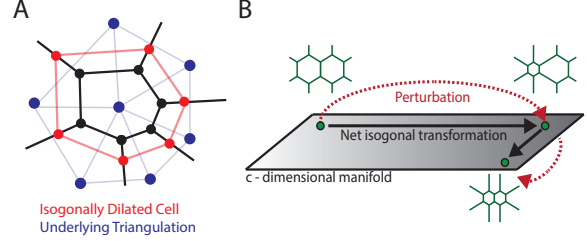


FIG. 4. (a) Cartoon illustrating the *isogonal*, i.e. angle preserving, breathing mode of a cell in a tension net. (b) A schematic diagram of expected ATN dynamics and the c -dimensional manifold of equilibrium lattice geometries. Transient perturbations take a cell array out of equilibrium, but because the equilibrium state is a manifold rather than a point, the system does not necessarily return to the same state, resulting in an ‘isogonal’ transformation.

zero around each cellular plaquette by hand

$$\sum_{\{\beta\}_\alpha} \mathbf{r}_{\alpha\beta} = 0 \quad \text{for } \forall \alpha \quad (12)$$

This is achieved by introducing Lagrange multipliers \mathbf{Q}_α for each cell in our original energy functional defined by Eq. (1). Interestingly, equilibrium values for Lagrange multipliers are equivalent to a $\pi/2$ rotation of our tension triangulation $\{\mathbf{Q}_\alpha^*\}$ defined above, modulo translations. Full dynamical equations for edge vectors can be derived analogously to Eq. (3), however we will only explore dynamics of small perturbations $\delta\mathbf{r}_{\alpha\beta}$ near equilibrium. In all equations that follow, time is rescaled $t \rightarrow \frac{t}{\nu}$ to reduce the appearance of unnecessary constants. The equations of motion are

$$\frac{d}{dt} \delta\mathbf{r}_{\alpha\beta} = -u_{\alpha\beta} \delta\hat{\mathbf{r}}_{\alpha\beta} - \hat{\mathbf{r}}_{\alpha\beta} \delta u_{\alpha\beta} + \delta\mathbf{Q}_{\beta\alpha} \quad (13)$$

where $u_{\alpha\beta} \equiv \kappa^{-1} T_{\alpha\beta}$ and $\delta\mathbf{Q}_{\beta\alpha} \equiv \delta\mathbf{Q}_\beta - \delta\mathbf{Q}_\alpha$. Lagrange multipliers are determined by imposing the constraint outlined by Eq. (12)

$$\sum_{\{\beta\}_\alpha} \delta\mathbf{Q}_{\beta\alpha} = \sum_{\{\beta\}_\alpha} [u_{\alpha\beta} \delta\hat{\mathbf{r}}_{\alpha\beta} + \hat{\mathbf{r}}_{\alpha\beta} \delta u_{\alpha\beta}] \quad (14)$$

Equation (14) can be thought of as Poisson’s equation for \mathbf{Q}_α defined over our dual triangulation, sourced by the out-of-equilibrium force summed around each cellular plaquette. It is convenient to project Eq. (13) into transverse and longitudinal components, defined by

$$\delta\mathbf{r}_{\alpha\beta} = \delta r_{\alpha\beta} \hat{\mathbf{r}}_{\alpha\beta} + \delta\theta_{\alpha\beta} r_{\alpha\beta} [\hat{\mathbf{z}} \wedge \hat{\mathbf{r}}_{\alpha\beta}] \quad (15)$$

leaving us with

$$\frac{d}{dt}\delta r_{\alpha\beta} = -\delta u_{\alpha\beta} + \hat{\mathbf{r}}_{\alpha\beta} \cdot \delta \mathbf{Q}_{\beta\alpha} \quad (16)$$

$$r_{\alpha\beta} \frac{d}{dt}\delta\theta_{\alpha\beta} = -u_{\alpha\beta} \delta\theta_{\alpha\beta} + \hat{\mathbf{r}}_{\alpha\beta} \wedge \delta \mathbf{Q}_{\beta\alpha} \quad (17)$$

The dynamics of small perturbations in intrinsic length is found by expanding Eq. (5) about the fixed point

$$\frac{d}{dt}\delta\ell_{\alpha\beta} = q_{\alpha\beta} [\delta u_{\alpha\beta} - \delta m_{\alpha\beta}] \quad (18)$$

where

$$q_{\alpha\beta} \equiv \frac{\nu\ell_{\alpha\beta}}{T_{\alpha\beta}} W'(1) \quad (19)$$

Tension dynamics is easily obtained via the constitutive relation defined in Eq. (4).

$$\begin{aligned} \frac{d}{dt}\delta u_{\alpha\beta} &= -(1 + q_{\alpha\beta})\delta u_{\alpha\beta} \\ &\quad + \hat{\mathbf{r}}_{\alpha\beta} \cdot \delta \mathbf{Q}_{\beta\alpha} + q_{\alpha\beta}\delta m_{\alpha\beta} \end{aligned} \quad (20)$$

Lastly, the myosin dynamics is governed by

$$\frac{d}{dt}\delta m_{\alpha\beta} = \omega (\delta u_{\alpha\beta} - \delta m_{\alpha\beta}) \quad (21)$$

where myosin has been rescaled to have units of interfacial deformation: $\delta m_{\alpha\beta} \rightarrow T_s \kappa^{-1} \delta m_{\alpha\beta}$ and $\omega \equiv \mu\nu\kappa^{-1} W'(1)$.

Isogonal modes correspond to $\delta\theta = \delta u = 0$ (and thus $\delta \mathbf{Q}_\alpha = 0$) which is realized by $\delta\ell_{\alpha\beta} = \delta r_{\alpha\beta}$, provided $\sum_{\{\beta\}\alpha} \delta r_{\alpha\beta} \hat{\mathbf{r}}_{\alpha\beta} = 0$. The latter constraint is satisfied for

$$\delta \mathbf{r}_{\alpha\beta\gamma} = \hat{\mathbf{r}}_{\alpha\beta} \frac{T_{\alpha\beta}\Theta_\gamma}{S_{\alpha\beta\gamma}} + \hat{\mathbf{r}}_{\beta\gamma} \frac{T_{\beta\gamma}\Theta_\alpha}{S_{\alpha\beta\gamma}} + \hat{\mathbf{r}}_{\gamma\alpha} \frac{T_{\gamma\alpha}\Theta_\beta}{S_{\alpha\beta\gamma}} \quad (22)$$

where $\delta \mathbf{r}_{\alpha\beta\gamma}$ denotes displacement of vertex at which adjacent cells α, β, γ meet and $S_{\alpha\beta\gamma}$ denotes the area of said vertex's dual triangular plaquette. Thus, isogonal deformations are parameterized by $\{\Theta_\alpha\}$ and have no restoring force. Tensions $T_{\alpha\beta}$ appear as coefficients because their ratios capture the implicit geometric constraints within tension nets central to the structure of the isogonal modes. (Note for example that $\delta \mathbf{r}_{\alpha\beta\gamma} = 0$ for $\Theta_\alpha = \Theta_\beta = \Theta_\gamma$.)

Equations (14, 16, 17, 20, 21) define the dynamics of fluctuations for ATNs near equilibrium. As the structure of these equations is quite complex, before presenting their full analysis we explore the more transparent case of a 1D linear chain before presenting their full analysis.

1. One-dimensional active tension cable.

In the limit of a one-dimensional uniform cable, $q_{\alpha\beta} = q$, Eqs. (16, 20, 21) reduce to

$$\frac{d}{dt}\delta r_i = \delta u_i - \delta u_{i-1} \quad (23)$$

$$\frac{d}{dt}\delta u_i = \nabla^2 \delta u_i - q(\delta u_i - \delta m_i) \quad (24)$$

$$\frac{d}{dt}\delta m_i = \omega (\delta u_i - \delta m_i) \quad (25)$$

where $\nabla^2 \delta u_i \equiv u_{i+1} + u_{i-1} - 2u_i$. Equations (24, 25) form a closed set which couples the dynamics of tension and myosin perturbations along the cable. Myosin does not appear in Eq. (23) and thus doesn't couple to tissue geometry directly. We consider the limit that $\omega \rightarrow 0$ and $\delta m \rightarrow 0$. Equation (24) is then recognized as the discrete form of a damped diffusion equation; a local perturbation of tension will diffuse through the linear array while cytoskeletal remodeling damps it to the stall condition over a time scale q^{-1} . From this and Eq. (23), we obtain the asymptotic change in length (in the continuum limit) of each actin bundle along the cable due to a perturbation of unit amplitude at the origin

$$\Delta r(x) = e^{-\sqrt{q}|x|} - \frac{2}{\sqrt{q}} \delta(x) \quad (26)$$

The entire process nets no change in tensions asymptotically, but locally remodels fiber lengths over distances of order $q^{-1/2}$, explicitly showing geometric plasticity. This is the 1D analog of the aforementioned isogonal mode. Relaxing the $\omega = 0$ constraint will only change the dynamics of u , opening up an acoustic branch that allows for the global rescaling of myosin and thus tension along the cable. However, as stated earlier, δm does not appear in Eq. (23) and thus plastic deformation will still occur, albeit now with a non-exponential profile (see S.I. for full analysis).

2. General two-dimensional case.

We now return to the general case of a 2D ATN. The equations of motion previously derived can be compactly written as the evolution of a $4e = 12c$ dimensional vector

$$\frac{d}{dt} \begin{pmatrix} \delta r_{\alpha\beta} \\ \delta u_{\alpha\beta} \\ \delta\theta_{\alpha\beta} \\ \delta m_{\alpha\beta} \end{pmatrix} = H_{\alpha\beta;\gamma\sigma} \begin{pmatrix} \delta r_{\gamma\sigma} \\ \delta u_{\gamma\sigma} \\ \delta\theta_{\gamma\sigma} \\ \delta m_{\gamma\sigma} \end{pmatrix} \quad (27)$$

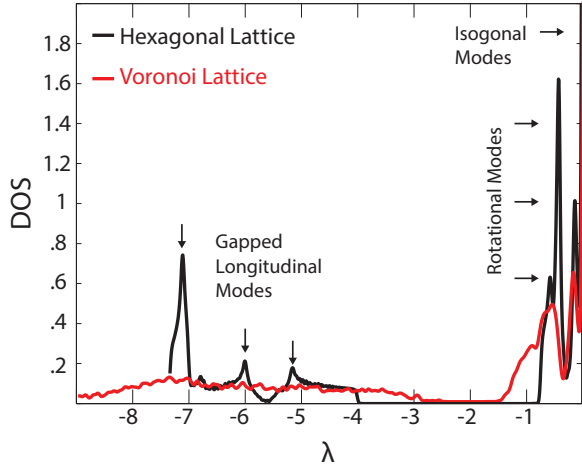


FIG. 5. “Density of states” plot for the normal modes of H governing the dynamics of fluctuations about the ATN equilibrium corresponding to i) a hexagonal array (black line) and ii) a randomly generated Voronoi tessellation (red line). For simplicity of visualization in both cases $\omega = 0$, which freezes out $3c$ modes, leaving $9c$ degrees of freedom. In both cases $3c$ modes lie at zero, including c isogonal modes and $2c$ geometric constraints (on edge vectors) constraints. The remaining eigenvalues are negative as required by stability. $1/3$ of the modes (in the hexagonal lattice case) are separated from zero by a gap proportional to the activity parameter q .

$H_{\alpha\beta;\gamma\sigma}$ is defined by Eqs. (14, 16, 17, 20, 21) and spelled out in the S.I. $H_{\alpha\beta;\gamma\sigma}$ has rank $9c$, reflecting the presence of $3c$ conserved quantities - the $2c$ constraints defined by Eq. (12) and c isogonal modes - that arise because longitudinal edge perturbations do not explicitly drive network dynamics. This is the 2D analog of the 1D actin cable wherein dynamics of edge lengths is slaved to the dynamics of tension and myosin. Each isogonal mode can be defined as a $12c$ dimensional vector, denoted ϕ_n^α where n labels the $12c$ components of the vector. Components are only non-zero along longitudinal perturbations $\delta r_{\alpha\beta}$, determined via Eq. (22) to be

$$\phi_n^\alpha = \begin{cases} -\frac{T_{\beta\gamma}}{S_{\alpha\beta\gamma}} & n = \beta\gamma \ \& \ \beta, \gamma \in \{\rho\}_\alpha \\ \sum_{\{\rho\}_\alpha \cap \{\rho\}_\beta} \frac{T_{\alpha\beta}}{S_{\alpha\beta\rho}} & n = \alpha\beta \\ 0 & \text{else} \end{cases} \quad (28)$$

$\{\rho\}_\alpha$ denotes the set of cells adjacent to cell α . In Eq. (22), a general isogonal transformation is defined by a set of parameters $\{\Theta_\alpha\}$ that specify the amplitudes of all ϕ^α eigenmodes. Conversely, the isogonal component of an arbitrary perturba-

tion is extracted by projecting the initial state vector $\mathbf{v} \equiv (\delta r, \delta u, \delta\theta, \delta m)^\top$ onto the ϕ^α eigenmode, $\Theta_\alpha = \sum_n \psi_n^\alpha v_n$, where ψ^α is the associated left eigenvector of H . It is defined by the condition $\sum_n \psi_n^\alpha \phi_n^\nu = \delta^{\alpha\nu}$ where ν indexes the set of *all* eigenmodes. As numerically demonstrated in the S.I., components along vertex and tension perturbations of ψ^α are found to be spatially extended within a length scale $q^{-1/2}$, centered about cell α . This is in direct analogy to the 1D cable, wherein length deformations are excited by tension perturbations within an exponentially localized patch of size $q^{-1/2}$.

Furthering the analogy to the 1D cable, we analyze the dynamics of the reduced system between δu , $\delta\theta$, and δm . The reduced matrix is manifestly symmetric in our chosen basis, and as we show in S.I., its eigenvalues are real and negative ensuring the system relaxes back to the same underlying dual graph. Fig. 5 illustrates the eigenvalue spectrum computed in the perturbation analysis of two cases: i) a regular hexagonal ATN state and ii) a highly disordered polygonal tiling state generated numerically as a random Voronoi lattice. For simplicity of presentation in Fig. 5, myosin dynamics is quenched by setting $\omega = 0$. Restoring myosin dynamics opens an acoustic branch that allows for global rescaling of tensions and for the dilation of the underlying triangulation, as found in the 1D cable limit. Perturbations in tension are again damped via cytoskeletal activity on the timescale set by q^{-1} , as evidenced by the scaling of their eigenvalues with q , shown in Fig. 5. These considerations reinforce the picture gleaned from both our graph-theoretic count and the 1D toy model - perturbations off the equilibrium manifold are damped by internal remodeling of the cytoskeleton, returning the system back to the same tension triangulation, but subsequently translating the system isogonally.

F. ATNs subject to external forces

We now study the response of an ATN to a small external force \mathbf{F} . The initial response is governed by linearized equations

$$\frac{d}{dt}\mathbf{v} = H\mathbf{v} + \mathbf{F} \quad (29)$$

and can be conveniently expressed by projecting onto the normal modes via $c^\nu \equiv \sum_n \psi_n^\nu v_n$ in terms of which

$$\frac{d}{dt}c^\nu = \lambda_\nu c^\nu + \sum_n \psi_n^\nu F_n \quad (30)$$

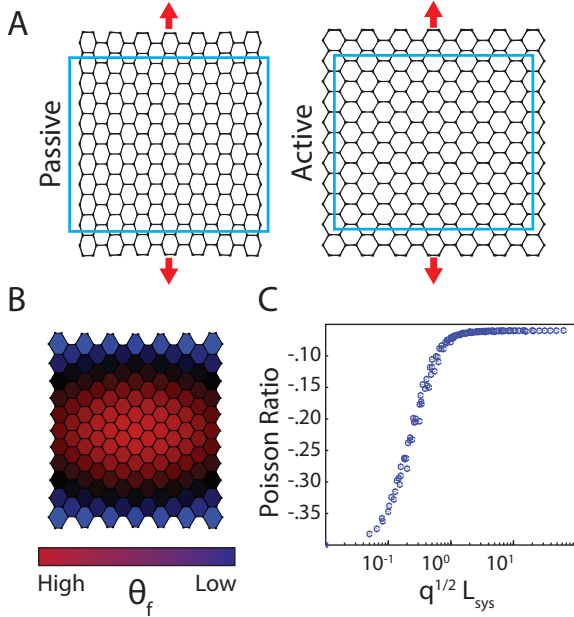


FIG. 6. (a) Negative Poisson ratio response. Diagrams of a passive ($q = 0$) and active ($q > 0$) network subjected to uniaxial tensile stress (red arrows). The blue box represents the initial state of the tissue. In response to the applied external force, the passive network shrinks along the orthogonal direction while the active network expands. (b) Distribution of Θ (see Eq. (28)) after re-equilibration in response to the uniaxial external force: the approximately parabolic profile implies excitation of a global dilation mode of the tissue. (c) Poisson ratio σ as a function of activity parameter q and tissue size L_{sys} (measured for a range of q and L_{sys} values) depends only on $q^{1/2} L_{sys}$. As external perturbations are screened within a length scale of $q^{-1/2}$, Poisson ratio approaches zero when $q^{1/2} L_{sys}$ exceeds one.

For isogonal modes $\nu = \alpha$ the eigenvalue is zero, $\lambda_\alpha = 0$, which implies secular growth of corresponding deformations with time, $c^\alpha(t) = t \sum_n \psi_n^\alpha F_n$, the growth rate being determined by the overlap of the corresponding left eigenvector with the external force field, projected onto the longitudinal component of each bond. The latter means that external forces are ‘screened’ within length scale discussed above - plastic deformation will be limited to a region of size $q^{-1/2}$. Of course this growth of deformation is not expected to continue indefinitely and is cut-off on the time scale of myosin redistribution, governed by Eq. (6), which will terminate the ‘slipping flow’ of acto-myosin bundles and thus re-equilibrate the tissue in the presence of the external

force. The plastic ‘isogonal’ deformation remains.

This raises an interesting question: how do isogonal modes change macroscopic mechanical properties of the epithelium in comparison to traditional passive materials? We focus on our model’s Poisson ratio σ , defined as the negative of the ratio of transverse to longitudinal strain in response to uniaxial stress applied on the boundary [36]. Passive networks generically have a positive Poisson ratio - they compress along the axis orthogonal to the applied tensile loads. Auxetic foams (materials with $\sigma < 0$) require concave cell configurations [37] and thus negative interfacial tensions to maintain force balance.

Interestingly, we generically recover $\sigma < 0$ for non-zero activity while still maintaining convexity of the underlying network. This is mediated by a global tissue dilation through the excitation of local isogonal modes via the external uniaxial force. For short times, isogonal modes roughly grow linearly with rate predicted by Eq. (31). Under uniaxial stress, these rates are patterned roughly parabolically - shown in Fig. 6(b) - resulting in an overall tissue dilation. The anisotropic distribution simply implies $|\sigma| < 1$. At long times, isogonal deformations are adiabatically quenched as myosin redistributes to triangulate the new boundary conditions. An important corollary to this picture is that σ should strongly depend upon the local contractility rate of the acto-myosin cytoskeleton; if the screening length $q^{-1/2}$ is on the order of the system size then the perturbation on the boundary will propagate the entire interior of the tissue and thus globally excite isogonal deformations. Conversely, if the screening length is much smaller than the tissue then most of the plastic deformation will be limited to a small layer around the stressed boundary and none along the orthogonal axis. This behavior was observed numerically for randomly generated Voronoi lattices, as shown in Fig. 6(d). Upon removal of the external force, the tissue was found to relax approximately back to the initial tension-triangulation and cell configuration. Interestingly, negative Poisson ratio has been observed experimentally for embryonic amphibian epithelia [38].

G. Ventral Furrow formation in *Drosophila* embryo

In the beginning of the gastrulation process in *Drosophila*, embryo cells along the ventral midline constrict their apical surfaces, initiating the formation of a furrow that subsequently internalizes the

future mesoderm [29], as shown in Fig. 7(a). This apical constriction was shown to be driven by pulsed contractions of a *medial* acto-myosin network (located on the apical cell surface) that connects to the adherens junction-anchored cortical cytoskeleton [39, 40]. The process has been described as a “ratchet” [39] where medial myosin pulses cause transient constrictions, that are subsequently stabilized by the retracted cytoskeletal cortex.

This phenomenon is readily interpretable in terms of our ATN model, which is a reasonable approximation because as shown in Fig. 2(c), embryonic epithelial cells appear to satisfy the geometric compatability constraint as defined by Eq. (9). We note that *medial* myosin pool exists in addition to the *junctional* myosin associated with the adherens junction-anchored cytoskeleton that is modeled by the ATN. If we assume that the junctional myosin concentrations are relatively static over the timescale of medial myosin pulsing, the ATN model predicts that any transient perturbation of mechanical balance due to medial myosin contractions would leave behind an isogonal deformation of the cell array, as it returns to mechanical balance dominated by cortical tensions that remain unchanged. Hence we predict that cell deformation during the early stages of ventral furrow formation should be well described by motion along an isogonal manifold.

This prediction was tested using time-lapse microscopy data on the early stage of Ventral Furrow formation in the *Drosophila* embryo [39, 40]. The initial time point of each movie was fit to the closest possible tension net, using the variational approach defined by Eqs. (10,11). Deformations of the cell array at subsequent time points were used to define the best fit amplitudes of isogonal modes. Specifically, Eq. (22) is a rectangular ($2v$ by c) linear system of equations defining vertex displacements corresponding to an arbitrary isogonal transformation $\{\Theta_\alpha\}$. Conversely, the best fit (in the sense of least square error) $\{\Theta_\alpha\}$ is given by a pseudo-inverse of this rectangular matrix. We found, as shown in Fig. 7(b), that thus defined isogonal modes accounted for about 90% of the total variance of the dynamic vertex displacement field, which clearly indicates that apical deformation of cells during ventral furrow formation is well approximated by an isogonal transformation. Thus, the cell array appears to behave much like a transiently perturbed ATN, flowing along the isogonal manifold which comprises the set of its (mechanical) equilibrium states. The latter, in turn, suggests that cortical-myosin levels do not significantly change during this time despite medial-myosin spiking. The results not only suggest that an

ATN model is suitable for describing tissue behavior, but also provide a simpler set of degrees of freedom that suitably describe the dynamics. The spatial distribution of final $\{\Theta_\alpha\}$ is shown in Fig. 7(c): It resembles parabolic cylinder straddling the ventral midline. The parabolic profile of isogonal mode amplitudes corresponds to anisotropic constriction of cells with the long axis oriented along the anterior-posterior direction [29].

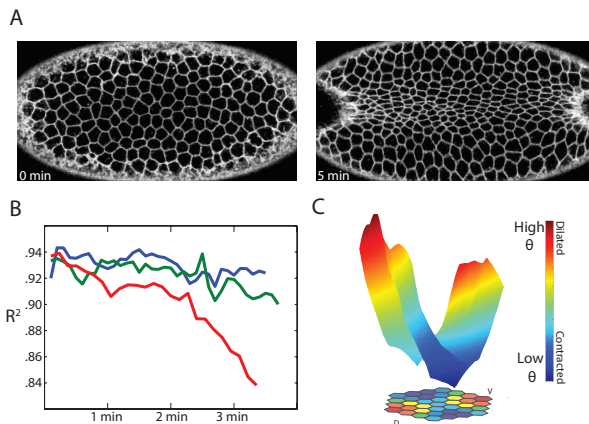


FIG. 7. (a) A ventral view of *Drosophila* embryo [40] at the beginning of Ventral Furrow formation process and just before the onset of invagination. (b) Fraction of the total variance for the experimentally measured vertex displacements captured by the best-fit isogonal transformation. Each color represents an independent time-course with approximately 50 cells. Good agreement was consistently found throughout. (c) Spatial profile of the isogonal mode amplitude, $\{\Theta_\alpha\}$, just before invagination. The approximately parabolic profile as a function of distance from midline describes progressively increasing and anisotropic compression of cells.

III. DISCUSSION

In this study, we proposed a quasistatic tension-dominated active model of epithelial tissue mechanics. There are two main assumptions on which this approximation rests: intercellular forces are dominated by cortical tensions held in the underlying actin network and that these tensions predominately balance each other across the tissue. Taken together, these assumptions make a falsifiable, quantitative prediction about the geometry of cells in static tension nets via our compatability constraint. This was subsequently tested against four different *Drosophila* epithelia. While perfect agreement was

neither found nor expected, the fact that three out of the four epithelia were found to cluster significantly closer to a static tension net as opposed to their empirically constructed “nulls” supports our original Ansatz. The formulated variational inference of interfacial tension should allow further and more direct tests our model once suitable experimental measurements of cortical tension became available.

Our study centers on the exploration of tissue-scale phenomena concomitant with internal cell remodeling. Specifically, our simple model, including only the effects of acto-myosin contractility and a generic load-dependent myosin walking rate, exhibited non-trivial, floppy ‘isogonal modes’ that are expected to dominate the dynamics asymptotically. This predicts local cellular plasticity excitable by both internal perturbations and external forces that decouples instantaneous stress and strain. This suggests a striking picture of tissue morphogenesis; we envision tissues operating in this limit to evolve their shape adiabatically, either by perturbing intercellular junctions to move isogonally, as shown to be the case for *Drosophila* ventral furrow formation, or via modulating cytoskeletal chemistry to excite movement off the isogonal manifold (see [41]). The existence of such zero modes makes quantitative predictions on macroscopic tissue behavior immediately amenable to experimental verification. For example, any such tissue should exhibit global auxetic behavior in response to uniaxial stress.

Isogonal modes can be thought of as the dis-

cretized degrees of freedom associated to the conformal symmetry of the continuum description. The elastic energy associated to displacement field u_i with vanishing bulk modulus is

$$E = \frac{1}{2} \int d^2\mathbf{r} [\partial_i u_k + \partial_k u_i - \delta_{ik} \partial_l u_l]^2 \quad (31)$$

Assuming relaxational dynamics - i.e. $\dot{u}_i = \frac{\delta E}{\delta u_i}$ - the equation of motion for field u_i is found to be $\dot{u}_i = -\partial^2 u_i$. Any solution of the Cauchy-Riemann equations can be added to u_i with no generation of additional internal stresses. That is to say, any conformal transformation of our equilibrium displacement field is also a valid ground state.

In conclusion, we expect that generalization of the ATN model and application of the proposed mechanical inference will further advance understanding of the interplay between cellular biophysics and tissue morphogenesis by making clear testable predictions that can be subsequently verified.

ACKNOWLEDGMENTS

The authors gratefully acknowledge numerous stimulating discussions with Ken Irvine, Thomas Lecuit, and Eric Wieschaus and would like to thank A. Martin and E. Wieschaus for sharing the Ventral Furrow data and K. Irvine for sharing the Wing Imaginal Disc data. This work was supported by the NSF PHY-1220616 (BIS) and by the GBMF grant #2919 (BIS/IH).

-
- [1] Bellaiche, Y. Heisenberg, C. (2013). Forces in Tissue Morphogenesis and Patterning. *Cell*, 153(5):948-962
 - [2] Farhadifar, R. Roper, JC. Aigouy, B. Eaton, S. Julicher, F. (2007). The influence of cell mechanics, cell-cell interactions, and the proliferation of epithelial packing. *Current Biology*, 17(24):2095-2104
 - [3] Rauzi, M. Verant, P. Lecuit, T. Lenne, PF. (2008). Nature and anisotropy of cortical forces orienting *Drosophila* tissue morphogenesis. *Nature Cell Bio*, 10:1401-10
 - [4] He B, Doubrovinski K, Polyakov O, Wieschaus E (2014) Apical constriction drives tissue-scale hydrodynamic flow to mediate cell elongation. *Nature* 508: 392-6.
 - [5] Lecuit, T. Lenne, PF. (2007). Cell surface mechanics and the control of cell shape, tissue patterns, and morphogenesis. *Nature MCB*, 8:633-644
 - [6] Nelson, C., Jean, R. Tan, J. Liu, W. Sniadecki, N. Spector, A. Chen, C. et al. (2005). Emergent patterns of growth controlled by multicellular form and mechanics. *PNAS*, 102(33):11594-9
 - [7] Shraiman, B. (2005). Mechanical feedback as a possible regulator of tissue growth. *PNAS*, 102(9):3318-3323
 - [8] Hufnagel, L. Teleman, AA. Rouault, H. Cohen, SM. Shraiman, B. (2007). On the mechanism of wing size determination in fly development. *PNAS*, 104(10):3835-40
 - [9] Fernandez-Gonzalez, R. Simeos, M. Roper, JC. Eaton, S. Zallen, J. (2009). Myosin II dynamics are regulated by tension in intercalating cells. *Dev. Cell* 17(5):736-43
 - [10] Gilbert S., 2000. *Developmental Biology*. Sinauer Associates, Sunderland.
 - [11] MacKintosh, F.C., Levine, A.J. (2008). Nonequilibrium Mechanics and Dynamics of Motor-Activated Gels. *Phys. Rev. Lett.* 100(1):018104
 - [12] Wang N, et al. (2002) Cell prestress. I. Stiffness and prestress are closely associated in adherent contractile cells. *Am J Physiol. Cell Physiol.* 282(3):C606616.
 - [13] Salbreux, G. Charras, G. Paluch, E. (2012). Actin

- cortex mechanics and cellular morphogenesis. *Cell* 22(10):536-545
- [14] Hartsock, A., Nelson, W. J. (2008). Adherens and Tight Junctions: Structure, Function and Connections to the Actin Cytoskeleton. *Biochimica et Biophysica Acta*, 1778(3), 660669. doi:10.1016/j.bbamem.2007.07.012
- [15] Hayashi, T., Carthew, R. (2004). Surface mechanics mediate pattern formation in the developing retina. *Nature* 431:647-652
- [16] Wozniak, M. Chen, C. (2009). Mechanotransduction in development: a growing role for contractility. *Nature MCB* 10:34-43
- [17] Kasza, K. Rowat, A. Liu, J. Angelini, T. Brangwynne, C. Koenderink, G. Weitz, D. (2007). The cell as a material. *Current Opinion in Cell Biology*, 19(1):101-107
- [18] Chiou, K. Hufnagel, L. Shraiman, B. (2012). Mechanical stress inference for two dimensional cell arrays. *PLOS Comp. Bio.*, 8(5)
- [19] Ishihara, S. Sugimura, K. (2012). Bayesian inference of force dynamics during morphogenesis. *J Theor Bio* 313:201-11
- [20] Honda, H. (1983). Geometric models for cells in tissues. *International Review for Cytology*, 81:191-248.
- [21] Landau, L., Lifshitz, E., 1987. Fluid Mechanics. Pergamon Press, Oxford. pp. 23839.
- [22] Marchetti, M.C., Joanny, J.F., Ramaswamy, S., Liverpool, T.B., Prost, J. Rao, M. Simha R., Hydrodynamics of soft active matter. *Rev. Mo. Phys.* 85(3):1144-1189
- [23] Mullens, R. Fletcher, D. (2010). Cell mechanics and the cytoskeleton. *Nature*, 463:485-492
- [24] Clemen, A. Vilfan, M. Jaud, J. Zhang, J. Barmann, M. Rief, M. (2005). Force-dependent stepping kinetics of myosin-V. *Biophys J.* 88(6):4402-10
- [25] Norstrom, M. Smithback, PA. Rock, R. (2010). Unconventional processive mechanics of non-muscle myosin IIB. *JBC* 285:26326-334
- [26] Kolomeisky, AB. Fisher, M. (2007). Molecular motors: a theorist's perspective. *Chem.*, 58:675-695
- [27] Campas, O., Kafri, Y., Zeldovich, K.B., Casademunt, J., Joanny, J.F. (2006). Collective dynamics of interacting molecular motors. *Phys. Rev. Lett.* 97(3):038101
- [28] Pouille PA, Ahmadi P, Brunet AC, Farge E. Mechanical signals trigger myosin II redistribution and mesoderm invagination in *Drosophila* embryos. *Sci Signal.* 2009;2:ra16.
- [29] Sweeton, D. Parks, S. Costa, M. Wieschaus, E. (1991). Gastrulation in *Drosophila*: the formation of the ventral furrow and posterior midgut invaginations. *Development*, 112(3):775-89
- [30] Bertet, C., Sulak, L., Lecuit, T. (2004). Myosin-dependent junction remodeling controls planar cell intercalation and axis elongation. *Nature*, 429:667-671
- [31] Calleja, M. Herranz, H. Estella, C. Casal, J. Lawrence P. Simpson, P. Morata, G. (2000). Generation of medial and lateral dorsal body domains by the pannier gene of *Drosophila*. *Development* 127:3971-3980
- [32] Milan, M. Campuzano, S. Bellido-Garcia, A. (1996). Cell cycling and patterned cell proliferation in the *Drosophila* wing during metamorphosis. *PNAS* 93:11687-11692
- [33] Maxwell J C. (1864). Relaxing in foam, *Phil. Mag.* 27 250
- [34] S. Henkes, C. S. O'Hern, and B. Chakraborty, (2007). *Phys. Rev. Lett.* 99, 038002
- [35] Boyd, S. Vanderberghe, L. (2004). Convex Optimization. Cambridge University Press
- [36] Landau, L., Lifshitz, E., 1970. Theory of Elasticity. Pergamon Press, Oxford. pp. 23839.
- [37] Yang, W. Zhong, M. Shi, W. Xie, B. Yang, M. (2004). On auxetic materials. *Journal of Materials* 39:3269-3279
- [38] Wiebe, C., Brodland, G.W., 2005. Tensile properties of embryonic epithelia measured using a novel instrument. *J. Biomech.* 38,20872094.
- [39] Martin, AC. Kaschube, M. Wieschaus, E.. (2009). Pulsed contractions of an actin-myosin network drive apical constriction. *Nature*, 457(7228):495-9
- [40] Martin, A., Wieschaus, E., Unpublished Data
- [41] Mani, M. Noll, N. Lecuit, T. Shraiman, B. (2015). Mechanochemistry in epithelial cell rearrangements and convergent extension. (Unpublished)